J Low Temp Phys
DOI 10.1007/s10909-013-0857-y

A Continuously Operating, Flux Locked, Superfluid Interferometer

Aditya Joshi · Richard Packard

Received: 22 November 2012 / Accepted: 18 January 2013

Abstract We report the characteristics of a flux locked, superfluid ^{4}He interferometer that can continuously measure time-varying rotation rates. We describe the principles underlying the interferometer, including the dynamics of a superfluid chemical potential battery used to obtain continuous operation. We also discuss noise and drift issues and their possible amelioration.

Keywords Superfluid · Interferometer · Gyroscope · Josephson effect

1 Introduction

Interferometers are used in many fields for measuring phase differences caused by a variety of physical influences. They have been constructed based on diverse wave phenomena ranging from the classical (light, sound) to the quantum (de Broglie matter waves—electrons, atomic beams, neutrons, Bose-Einstein condensates and superfluids).

While DC superfluid helium quantum interference devices (SHeQUIDs) using ^{4}He are relative newcomers to interferometry, they have been steadily increasing in sophistication since their debut in 2005. In recent years, a series of proof-of-principle experiments have demonstrated various operational aspects of SHeQUIDs. In this paper, we put most of these functions together to achieve continuous operation while using flux locking to linearize this intrinsically non-linear device.

A. Joshi (✉) · R. Packard
Department of Physics, University of California, Berkeley CA 94720, USA
e-mail: adityaj@berkeley.edu

R. Packard
e-mail: rpackard@berkeley.edu

Published online: 26 January 2013

2 SHeQUID Basics

The SHeQUID utilizes coherent oscillations that occur when a chemical potential difference is impressed across an array of nanoscale apertures. The physics of this "quantum whistle" and the working of the SHeQUID are described and referenced in Ref. [1]. Briefly, a chemical potential difference $\Delta\mu$ across a nanoscale aperture array [2] that acts as a barrier between two superfluid volumes, creates a coherent mass-current oscillation through the array with a frequency $f_J = \Delta\mu/h$ (where h is Planck's constant) via either the Josephson current-phase relation or coherent phase-slippage [3]. We detect this quantum whistle by coupling the fluid to a flexible diaphragm whose motion is monitored with a sensitive displacement transducer [4].

Arranging two of these aperture arrays in the topology of a loop (see Fig. 1) yields two whistle sources with distinct quantum phases. These can combine and interfere to produce an observable oscillation whose amplitude is cosinusoidally modulated by the difference in phase drops $\Delta\phi \equiv \Delta\phi_1 - \Delta\phi_2$ between the two whistles. Consequently, in a SHeQUID, changes in the phase are deduced from changes in the oscillation amplitude.

The phase difference $\Delta\phi$ can be affected by several different physical phenomena —essentially, effects that couple to the order parameter phase of a neutral matter condensate. Demonstrated examples include coupling to a physical rotation (the Sagnac effect [5, 6]) and the counterflow caused by a heat current down a channel [7]. Superfluid velocity is equivalent to a gradient in the phase of the superfluid order parameter according to the relation $v_s = (\hbar/m_4)\nabla\phi$ (where m_4 is the mass of a ^{4}He atom), so

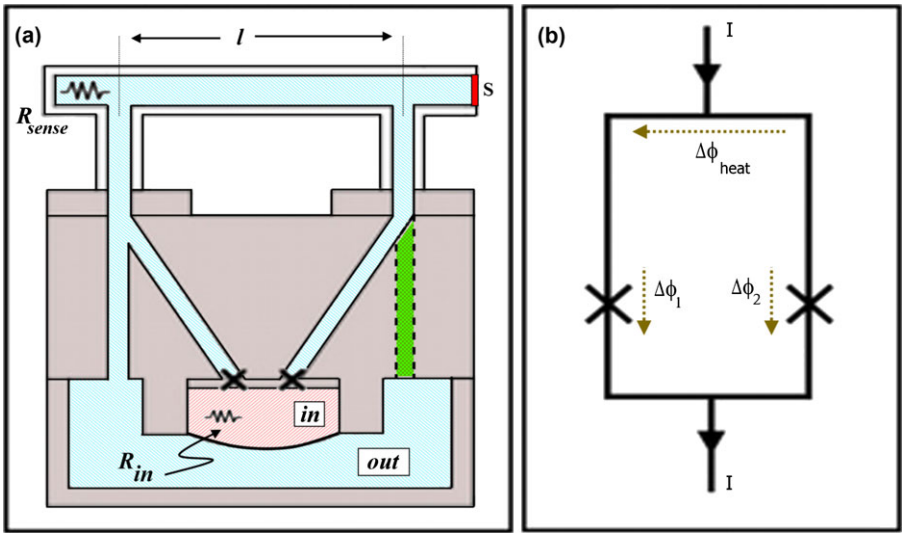

Fig. 1 (**a**) Cell schematic and (**b**) equivalent circuit (dotted arrows denote the direction of increasing phase for the phase-drops shown). Resistive heater (R_{sense}) and roughened copper-foil sink (S) in the top "heat-pipe" produce a superfluid counterflow from S to R_{sense}. This is equivalent to a phase-difference $\Delta\phi_{heat}$ between the two vertical side arms (and thus between the two aperture arrays marked X). The darker, dashed flow path (*green online*) shown does not exist yet—it is a feature considered for future versions as a possible way to ameliorate the heat-pipe drift as described in Sect. 10 (Color figure online)

that a SHeQUID can be thought of, at its heart, as a highly sensitive detector of superflow velocities. Effects that change a superfluid velocity can be detected and measured by this device.

As shown in Ref. [8], the resultant (measured) oscillation amplitude I_t is a non-linear function of the relative phase difference $\Delta\phi$ between the two apertures and is given by:

$$I_t = a\left[\cos^2\frac{\Delta\phi}{2} + b\sin^2\frac{\Delta\phi}{2}\right]^{1/2} \tag{1}$$

where I_1 and I_2 are the individual oscillation amplitudes in each aperture array, $a = (I_1 + I_2)$ is the maximum observed amplitude, and $b = (\frac{I_1 - I_2}{I_1 + I_2})^2$ describes the asymmetry between the two aperture arrays. For the scenario presented in Fig. 1(b), $\Delta\phi \equiv \Delta\phi_1 - \Delta\phi_2 = \Delta\phi_{heat} + \Delta\phi_{ext} + \Delta\phi_{offset}$, where $\Delta\phi_{heat}$ is a phase-shift due to a heat current in one leg of the interferometer, $\Delta\phi_{ext}$ is any other externally imposed phase-shift (such as $\Delta\phi_{rot}$—the phase-shift from rotation, which is discussed in Sect. 5) and $\Delta\phi_{offset}$ is any constant phase offset (due to, for instance, trapped circulation in the sense loop). As we will see in Sects. 5 and 6, this function fits well the interference curves observed by varying different phase-shifting influences.

3 The Chemical Potential Battery

The chemical potential difference $\Delta\mu$ depends on both pressure and temperature differences, ΔP and ΔT as $\Delta\mu = m_4(\Delta P/\rho - s \cdot \Delta T)$, where ρ is the total density and s is the entropy per unit mass of helium [9]. Therefore, unbalanced ΔP or ΔT terms can both result in a non-zero $\Delta\mu$ (and thus a whistle with frequency $f_J = \Delta\mu/h$). In previous versions of the SHeQUID (used as a rotation sensor), the quantum whistle was generated by the application of a pressure step ΔP [10] or a temperature step ΔT [11]. However, the frequency of these whistles decays to zero over time, mirroring a decay in $\Delta\mu$. The dissipation mechanism is briefly described below for two different whistle excitation methods. We show here how the second method can be modified to obtain continuous oscillations.

When a pressure step ΔP is applied across the aperture array by electrostatically pulling on the diaphragm, a quantum whistle is observed with a frequency that decays over time (due to a $\Delta\mu$ that relaxes over time). $\Delta\mu$ relaxes both due to net fluid flow into the cell causing ΔP to relax as well as due to net *superfluid* flow inducing a ΔT that reduces the magnitude of $\Delta\mu$. We can delay this relaxation for a few seconds by continuously increasing the pull on the diaphragm (applying more and more ΔP) to keep f_J constant (i.e. using a feedback routine on f_J).

When a heater power $\dot{Q}_{IN}$ into the inner cell is stepwise increased, the temperature of the fluid inside the inner cell begins to rise, creating a temperature difference ΔT across the aperture array (and therefore a $\Delta\mu$). Josephson oscillations are observed, beginning at a low frequency, which begins to increase together with ΔT. Heat is carried out of the inner cell by the normal current I_n and conduction through the cell walls. $\Delta\mu$ drives a net DC supercurrent I_s into the cell, causing a pressure difference ΔP to build, which counteracts the ΔT term in the expression for $\Delta\mu$. The Josephson

frequency ($\propto \Delta\mu$) thus rises to a maximum and drops again as the ΔP term catches up to the ΔT term. Equilibrium is reached when this process brings $\Delta\mu$ down to 0 and ΔP reaches a steady "Fountain pressure" given by $\Delta P = \rho s \Delta T$. At steady state, the net current is $I_t = I_n + I_s = 0$ (so that $I_n = -I_s$ where these are time-averaged, DC values of the currents) and the heater power injected into the cell is balanced by heat flowing out of the cell via the normal flow and wall conduction [11].

The whistles created this way are therefore transitory and typically decay in a few seconds (in temperature regimes where the signal is high enough to provide good sensitivity). This transient method of monitoring a phase difference is not optimal since it involves a low duty cycle and requires measuring the amplitude of a continuously changing oscillation frequency. The feedback technique described above (for the pressure-step excited whistle) works in prolonging the whistle transient but the limited feedback dynamic range is such that it has to be reset often (see Ref. [12] for limit details). Due to the low duty cycle of the transient methods, the S/N and the response time are compromised.

A continuous whistle needs a different technique—the so-called chemical potential battery [13, 14]. If the cell heater power $\dot{Q}_{IN}$ (in the previously described scenario) is increased, the quantities I_s, I_n, ΔP and ΔT all increase towards trying to maintain $\Delta\mu = 0$ in the final steady state. But the supercurrent I_s cannot exceed a critical current I_c. This puts an upper bound on the DC supercurrent and consequently, (in steady state) on the normal flow as well, both of which govern the whistle dissipation. Increasing $\dot{Q}_{IN}$ beyond this critical point therefore leads to a steady state where $\Delta\mu > 0$ and the Josephson oscillations occur continuously without any further decay in frequency. This constitutes a chemical potential "battery" and this state will henceforth be referred to as a "battery state". In an ideal case, we would be able to conveniently change $\Delta\mu$ by adjusting the heater power in order to set the whistle frequency to arbitrary values. The reality is more complicated and involves phenomena that we describe in the following section.

4 Resonant Locking—Attractors and Repulsors

The cell supports several hydrodynamic resonant modes, which are essentially standing waves in various cavities. The interaction of a battery state with these resonances involves physics analogous to the Fiske effect in superconducting weak links [15]. During the cell heater ramp-up, when the battery frequency approaches a cell resonance, homodyne mixing of the resonant mode with the whistle provides an additional DC current [16], which could be flowing either into or out of the inner cell, depending on the relative phase between the two oscillations. This is because the DC current enhancement is proportional to the sine of the relative phase [17], which can be positive or negative. This current combines with the battery driven flow to (respectively) accelerate or retard the battery state's progress in frequency space towards the resonant mode during the heater ramp. The two cases then lead to either an attractor or a repulsor in frequency space.

We have investigated the resonant modes of our cell below 4 kHz. We can determine some of the cell resonances by exciting the cell with an electrostatically applied

harmonic force while monitoring the displacement transducer response. The resonant frequencies we observe with this method are battery repulsors and do not seem to match the many battery attractors seen.[1] This may be strongly cell dependent, as Sato, *et al*. found no repulsors and observed attractors at a mix of identified/unidentified cell resonant frequencies.[2] This is not surprising since the relative phases that determine the sign of the extra DC superflow would depend on cell dimensions and specific details of node/antinode locations of the resonances.

The attractor cell resonances have the twin advantages of locking the battery at a resonant state with excellent stability and significantly amplifying the whistle amplitude. The unfortunate aspect of the cell resonances is that the resonant amplification (referred to henceforth as the "Fiske gain") is strongly frequency dependent. For example, the interference patterns in Fig. 2 and Fig. 3 were taken at the same temperature but used different battery states (1080 Hz and 2507 Hz respectively) and have maximum amplitudes of 29 and 55 ng/s owing to the differing Fiske gains. We explore the implications of this issue in Sect. 9.

These resonant phenomena also lead to complex hysteretic behavior, where the equilibrium battery frequency attained depends not only on the inner cell heater power $\dot{Q}_{IN}$ but also on the details of the path followed to get to that value. We are thus far unable to predict the spectrum of battery frequencies $f(\dot{Q}_{IN})$ as such an analysis requires a more detailed understanding of the cell dynamics. We note that none of these nonlinear mixing and hysteresis effects prevent one from actually using these phenomena for practical purposes, though an improved understanding would undoubtedly enable even greater ease of operation. For instance, being able to engineer a sharp, resonant attractor in an otherwise clean frequency regime would simplify the techniques used and improve stability.

5 Continuously Operating SHeQUID as a Gyroscope

The Fiske amplified chemical potential battery thus enables continuous operation of the SHeQUID with the added bonus of improving the signal as well as the phase sensitivity [12]. In Fig. 2, we show the measurement of a continuously varying rotational flux using such an enhanced device—the first of our two main results in this paper. The data in this figure were obtained by a continuous (as opposed to point-by-point[3]) reorientation of the SHeQUID in the rotating reference frame of the Earth. To obtain the data in Fig. 2, we capture short (∼80 ms long) timeseries of the position of the diaphragm. For each time segment, we perform a Fast Fourier Transform (FFT) to obtain the frequency spectrum and then integrate the whistle peak (at about 1080 Hz

[1] One exception to this rule is the so-called Helmholtz mode (the fundamental mode for small oscillations of the superfluid in the apertures), which does behave as an attractor.

[2] Y. Sato, personal communications (pertaining to experiments in Ref. [12]).

[3] See Sect. 9 for a discussion on issues related to such continuous reorientation.

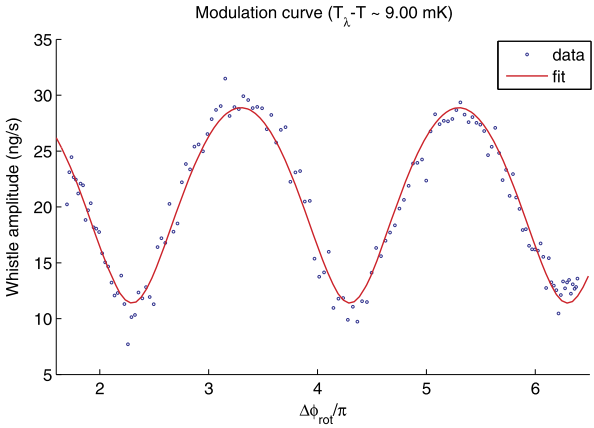

Fig. 2 Interference from continuously reorienting the SHeQUID. This changes the rotation flux incident on the sense loop (and thus the relative phase difference between the aperture arrays). Data taken as described in Sect. 5 is bin-averaged for every 1° of dewar rotation before plotting (Color figure online)

in this case[4]) to find the whistle amplitude I_t. Automated Labview[5] programs do this continuously so that we have an almost real-time measure of I_t.

The expression for the Sagnac phase-shift [5, 6] is,

$$\Delta\phi_{rot} = (4\pi m_4/h)\vec{\Omega}\cdot\vec{A} \tag{2}$$

where Ω is (in this case) the Earth's angular velocity ($\sim 7.29 \times 10^{-5}$ rad/s) and $\vec{A}$ is the area vector of the interferometer sense loop. In our apparatus $\vec{A}$ is oriented horizontally so that when the SHeQUID is reoriented, the vector sweeps out a circle in a plane parallel to the ground. In terms of angular position θ of the cryostat (on which the SHeQUID is rigidly mounted), Eq. (2) becomes:

$$\Delta\phi_{rot} = 2\left[(2\pi m_4/h)\Omega A\cos\lambda\right]\cos(\theta-\theta_0) \equiv 2c_{rot}\cos(\theta-\theta_0) \tag{3}$$

where λ is the latitude of the location of the experiment (37.9° north in this case) and θ_0 is the cryostat position for which $\vec{A}$ points due North (or South). θ is measured from an arbitrary reference zero using a commercial digital angle indicator[6] whose resolution is ~0.1°. The expression for current (Eq. (1) with $\Delta\phi_{rot}$ from Eq. (3)) is fit to the data to obtain c_{rot} as a fit parameter. Using Eq. (3) and the known values of λ and Ω, we can obtain the effective area A of the sense loop (~10.9 cm^2), which differs from the design value by ~2 %. The design value (~10.7 cm^2) is the area of the loop defined by the axial paths along all tubular elements in Fig. 1(a) (which should be close to the averaged path "seen" by the superflow [18]). We see that the axial path is a good approximation to the effective boundary of the sense loop.

[4]The duration of a timeseries chunk is chosen to be long enough to include several tens of whistle cycles for accurate FFT results and can be made smaller when the battery state is dialed higher in frequency.

[5]National Instruments Labview software.

[6]Renco Encoders Inc. model E-series optical encoder.

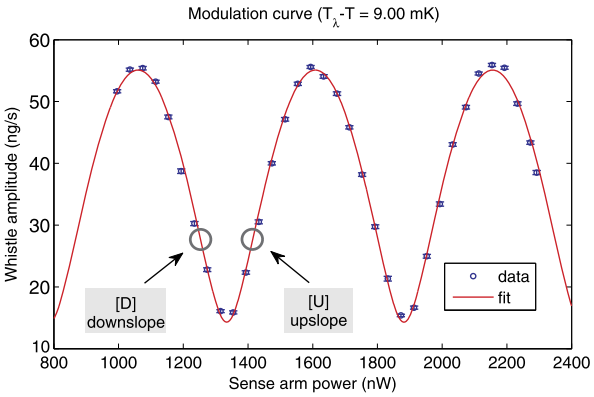

Fig. 3 Interference pattern obtained by sweeping the heat-pipe power (proportional to phase), as described in Sect. 6. The two types of biasing points of steepest slope are marked U (upslope) and D (downslope) (Color figure online)

6 Flux Locking and Linearization

The main idea with flux locking is to use a heat-induced phase shift to counteract the rotation-induced (or otherwise externally influenced) phase shift, thereby keeping the phase (and therefore the whistle amplitude) constant. The element used for flux locking is the heat-pipe shown in Fig. 1 and described in more detail in Ref. [8]. A power $\dot{Q}$ injected into the heat-pipe heater R_{sense} creates a counterflow in the heat-pipe, with the superfluid flowing towards the heater and normal fluid carrying heat away from it, towards a thermal sink S (a thin, roughened copper sheet). The phase difference $\Delta\phi_{heat}$ induced between the interferometer arms due to this counterflow is given by [8]:

$$\Delta\phi_{heat} = 2\left[\frac{l}{\sigma}\frac{\pi m_4}{h}\frac{\rho_n}{\rho\rho_s T s}\right]\dot{Q} \equiv 2k_h\dot{Q} \tag{4}$$

where ρ_n and ρ_s are the normal and superfluid densities respectively, T is the temperature in the cell, l is the spacing between the arms and σ is the cross-sectional area of the heat-pipe.

Figure 3 is an example of an interference pattern obtained by sweeping the heat-pipe power. We have fit the same functional form to this data as we did for Fig. 2, except with $\Delta\phi_{heat}$ from Eq. (4) instead of $\Delta\phi_{rot}$. This fit yields the fit parameters a, b and k_h, where k_h is related to the change in heat-pipe power ($\dot{Q}_{2\pi} = \pi/k_h$) needed to make a 2π phase-shift across the sense arm. If we compare the fit value of k_h to the theoretical value from Eq. (4), we find that they agree within $\sim$1.4 % (the main source of systematic error being the effective length l, which is affected by flow details at the tube intersections [19]).

From Eq. (4), we see that the amount of heat-pipe power required to hold the SHeQUID at a point of constant phase is a linear measure of the rotationally induced phase-shift. The parameter k_h provides a calibration for this device by translating heater powers to phase-shifts, while a and b are used to optimize the automated flux-locking routine described in the following section.

7 Feedback

Previously [8], we demonstrated a static, point-by-point feedback as proof of principle. In that work, the cryostat was initially oriented so that the SHeQUID was biased at one of the points of steepest slope in Fig. 3 and the average amplitude recorded. The cryostat was then reoriented to a new position, thus changing the Sagnac phase. The heater power in the heat-pipe was then manually changed to bring back the amplitude to its original value. This process was repeated for many angular positions. The feedback input (heat-pipe power) was shown to depend linearly on the Sagnac phase. Such a method is of limited utility for monitoring time-varying rotation signals unless such variations are extremely slow. One of the main products of the present work is an automated computer system that can generate a battery state, perform a calibration, assist in optimal biasing and finally, adjust the feedback output power in response to the external phase changes that we wish to track. The process is as follows:

1. Once a stable battery state (with acceptable Fiske gain) is obtained, the computer program calibrates the device (as described in Sect. 6) and obtains the parameters a, b and k_h.
2. For the device to have sufficient dynamic range to track (+) and (−) phase shifts, the system must be able to add or remove heater power from the heat-pipe. Therefore, we impose an initial power offset of several 2π cycles (a few μW of power here).
3. The operating point (of maximum phase sensitivity) is found by adjusting the power offset until the amplitude is equal to the value at the steepest points in Fig. 3 ($I_{S\max} = b^{1/4}a$ from Eq. (1)).
4. The whistle amplitude is now continuously measured and the change in whistle amplitude δI between consecutive measurements constitutes the "error signal" in a proportional feedback scheme. This is used to compute the heat-pipe feedback power adjustment required to nullify the error. At the steepest point, this is $\delta\dot{Q} \approx \delta I \cdot (dI_t/d\dot{Q})^{-1}_{\max} = \delta I \cdot [a(1-\sqrt{b})k_h]^{-1} \equiv \delta I \cdot G_0$, with G_0 being a good initial value for the proportional gain.[7] We record the total heat-pipe power in each iteration of the feedback loop and this is our feedback output signal $\dot{Q}_{FB}$.
5. The total phase seen by the SHeQUID given both rotation and heater power is $\Delta\phi = \Delta\phi_{heat} + \Delta\phi_{rot} + \Delta\phi_{offset}$. If the total phase is kept constant using feedback, we should observe that $\Delta\phi_{heat} = -(\Delta\phi_{rot}) + \text{constant}$. We use the feedback power $\dot{Q}_{FB}$, calibration k_h and Eq. (4) to compute $\Delta\phi_{heat}$. Together, they constitute the measured phase-shift. The dewar angular position (independently recorded during the feedback run) and c_{rot} obtained from the fit to Fig. 2, are used with Eq. (3) to compute the actual Sagnac phase-shift $\Delta\phi_{rot}$. We plot $\Delta\phi_{heat}$ vs. $\Delta\phi_{rot}$ in Fig. 4 and see that our SHeQUID is indeed, continuously tracking the Sagnac phase correctly (with a systematic error of ∼1 %). This is the second main result for this paper.

[7] In practice, about half this value seems to work well to avoid feedback oscillations.

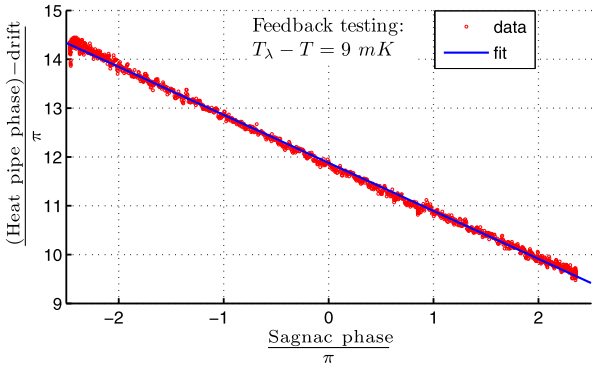

Fig. 4 Example of dynamic feedback demonstration in a continuously operating SHeQUID. The expected slope is −1 (see feedback process step 5 in Sect. 7). The slope of a linear fit to the data is −0.98. The fit vertical intercept corresponds to ∼7 cycles of heat-pipe offset, plus the phase required to bias at the steepest point (see feedback process steps 2 and 3 in Sect. 7). Phase drift has been subtracted from the data (see Sect. 10) (Color figure online)

8 Performance

8.1 Noise

The current noise δI_n is calculated as the standard deviation of the mean of the whistle amplitude measurements in a single iteration of the feedback loop. By biasing the device at the steepest part of the interferogram, we can measure the noise in the system with the greatest sensitivity. We obtain the phase noise $\delta\phi_n$ (in rad) from the current noise δI_n by using the phase sensitivity at the steepest point S_m (measured from a sample interferogram): $\delta\phi_n \approx \delta I_n \cdot (dI_t/d\Delta\phi)^{-1}_{\max} \equiv \delta I_n / S_m = \delta I_n \cdot [a(1 - \sqrt{b})/2]^{-1}$, which is then normalized to one second of measurement time to obtain the phase noise density (PND).

For the flux locked device reported here, we find a PND of 9×10^{-2} rad/$\sqrt{\text{Hz}}$ at our operating temperature of 9 mK below T_λ. The noise limitation is due to fluctuations in the SQUID-based displacement sensor that are an order of magnitude greater than the intrinsic noise in the SQUID. By comparison, the best-quoted phase noise in a Fiske-enhanced SHeQUID [12] is 3×10^{-3} rad/$\sqrt{\text{Hz}}$ and in a multi-turn device [20] is 3×10^{-2} rad/$\sqrt{\text{Hz}}$.

8.2 Response Time and Slew Rate

This is ultimately determined by the time required to determine the amplitude of the quantum whistle. It takes us on the order of a second to acquire sufficient data for this purpose in each iteration of the feedback loop.

We can define the slew rate of this device (in the same manner as that for SQUIDs) as the maximum rate of phase change that the feedback can track without losing lock. While the intrinsic slew rate for this device is presently unknown, we observed that

the feedback could maintain lock for phase change rates up to a maximum[8] value of 20 mrad/s). The phase change rate is $\dot{\Delta\phi} = -(4\pi m_4/h)A\cos\lambda[\Omega\dot{\theta}\sin(\theta-\theta_0)]$, which is just the time derivative of Eq. (3). This formulation allows us to see more explicitly that a *constant* cryostat reorientation rate $\dot{\theta}$ imposes *time-varying* phase change rates upon the sense loop during a continuous reorientation. If we interpret the quantity in square brackets as an effective angular acceleration (as seen by the sense loop), we can restate the limit stated above as a maximal angular acceleration of $\sim$180 nrad/s^2 that the feedback has been shown to successfully track.

8.3 Dynamic Range

This is set by the usable range of heat-pipe power values. As observed in Ref. [21], when one increases the heat-pipe power above a critical value, the superflow in the pipe becomes turbulent and vortices crossing the pipe cause the SHeQUID phase to oscillate through 2π. For the heat-pipe used in Ref. [21], the dynamic range actually observed corresponded to a phase-shift of $\sim 250 \times 2\pi$. We note that the heat-pipe dimensions and heater powers used in this work are nearly identical to the ones used in Ref. [21] and also in a further experiment where this dynamic range was subsequently verified.

Since the sensing points (the two vertical side-arms in the sense loop) are designed to be far from the ends of the heat-pipe, we have observed only a linear relationship between heater power and the phase response (up to the turbulent limit). Non-linearity considerations come into play only for multi-path interferometers (such as the 4-path "grating" interferometer described in Ref. [22]) where small differences in distances between the sensing points get amplified with increasing heater power and distort the interferogram. For the single-loop SHeQUID in the present work, linearity is not a problem.

9 Continuous Reorientation with a Simplified Bearing

In all our previous work, the SHeQUID loop vector $\vec{A}$ was reoriented point-by-point to change $\Delta\phi_{rot}$. This was done because our previous reorientable cryostat included homemade hydraulic or pneumatic bearings that injected considerable noise into the system. This noise increased the base noise level of the displacement sensor (reducing sensor resolution) and also interfered with temperature regulation during rotation. Consequently, the bearings had to be turned off during a measurement.

The situation was exacerbated while using the chemical potential battery due to its hysteresis. The bearing noise and the large temperature fluctuations caused by it would often knock the battery state to nearby stable or (worse) metastable states. Because of the frequency dependent Fiske gains associated with each battery state,[9]

[8] We can call this a lower bound for the effective slew rate for this device at the present time, since this maximum value occurs during the fastest cryostat reorientation rate ($\sim$9 deg/min) that we have been able to sustain under the temperature regulation and battery stability constraints noted in Sect. 9.

[9] See Sect. 4 for details.

we might now be tracing out a different interference curve. Such amplitude gain jumps are intolerable since all we can do in practice during the feedback is keep the amplitude at a fixed value. Whether a fixed amplitude means a fixed phase depends on our ability to stay confined to one interference curve out of the family of curves corresponding to the nearby battery states. The SHeQUID feedback calibration is thus frequency dependent (at least in a system with the many cell resonances that we observe) and any battery fluctuations or jumps can render it useless and the feedback unusable. A future improvement to the SHeQUID might be an additional feedback system that kept the battery state fixed by small, occasional adjustments to the inner cell heater power.

For these reasons, we built a quieter rotation stage that employed a simple commercial ball bearing[10] rather than the previously used fluid bearings. This new rotation stage injects no observable noise into the temperature regulation system,[11] thus allowing the maximum stability of ∼20 nK. This is an almost 1000-fold improvement in thermal stability during rotation.

10 Parasitic Drifts

To be most useful as a continuous monitor of long-term changes in some parameter (e.g. small changes in the Earth's rotation rate), it would be best to have no intrinsic long-term drifts in the SHeQUID. At temperatures further below T_λ, ever greater heater power is required in the inner cell to reach the critical velocity and generate a continuously whistling battery state. We find that when $\dot{Q}_{IN}$ is on the order of microwatts, the SHeQUID phase drifts noticeably over time. We have measured this drift as a function of time and temperature during several different runs, each run consisting of the ∼2 day period after transferring liquid helium into our cryostat. A sample drift run is shown in Fig. 5(a) and the results of the entire series of drift runs are summarized in Fig. 5(b).

From these drift measurements, we note two significant features: (1) there is a clear decrease in drift rates with decreasing inner cell powers (correspondingly being closer to T_λ); and (2) the drift rate in each run decreases smoothly in time, dropping by about a factor of two over a period of 48 hours. This drift (measured independently of the feedback) has been subtracted from the data shown in Fig. 4. The feedback test in Fig. 4 was performed at 9 mK below T_λ at ∼7.5 inches of bath level where the drift rate (of ∼30 nW/hr) was fairly constant over the duration of the test of ∼1 hr (compare that to over 1200 nW of feedback output change during the same period of time).

We verified that this drift does not come from drifts in the heat-pipe power by shorting the resistive heater in the heat-pipe during some drift runs (instead, obtaining families of plots like Fig. 2 by sweeping the cryostat angular position back and forth).

[10] BearingsOn UCF215-48 flange-mounted 3 inch diameter bearing.

[11] Up to some maximum cryostat rotation rate on the order of tens of deg/min, which is determined by the specifics of the experiment (cabling, weight distribution, etc.).

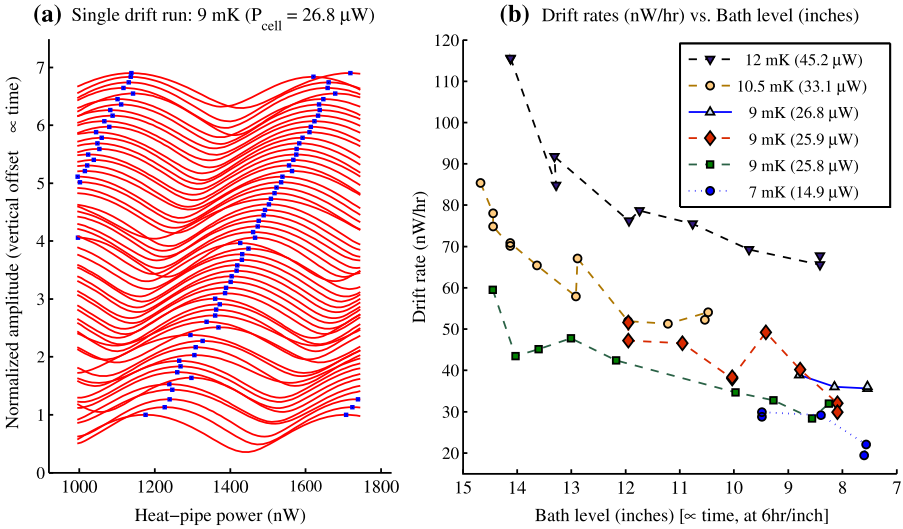

Fig. 5 (**a**) Plots from a representative drift run described in Sect. 10. Each plot is a fit (of Eq. (1)) to an interferogram created by sweeping the heat-pipe power back and forth between two extreme values. The fit result amplitude is normalized (so that we can focus solely on the phase information) and the curves are plotted with approximately equal vertical offsets (proportional to the actual time of each sweep) with an average duration of ∼12.8 min between sweeps. The locations of the maxima (shown as *solid squares*) can then be used to obtain the rate at which the phase is drifting. This is done by binning the maxima location data over time and finding slopes in each bin. (**b**) This drift rate is observed to vary over time and with temperature (in mK below T_λ), which also dictates the inner cell heater power needed for the battery. We have plotted drift rate data from several drift runs against the helium bath level (which is proportional to time at ∼6 hr/inch). We can see that the drift rates decrease with time (and bath level) as well as with inner cell heater power (included parenthetically in the figure legend) (Color figure online)

Thus far, we have not discovered the mechanism of the cell heater dependent drift in the present apparatus. However, we suspect that some of the inner cell heater power leaks into the heat-pipe, the leakage amount drifting as the Dewar's liquid helium level falls. We do not have a detailed model of the heat flow out of the inner cell but some of the heat must be transferred to the surrounding bath and some may leak into the heat-pipe. If the ratio of these two conductance paths changes in time, it would cause a drift in the interferogram.

We hope to make changes in a future apparatus that would eliminate this possibility (or at least reduce its impact). Specifically, adding a second, symmetric return path to the SHeQUID loop (the darker, dashed, vertical flow path—colored green online—shown in Fig. 1(a)) or converting both return paths into superleaks might remove the unbalanced conductance path leading from the inner cell to the heat-pipe. An additional helium-filled, temperature regulated, sealed enclosure around the cell might prevent a time variation in heater power flowing from the inner cell to the heat-pipe. The smallest drift rate seen in an independent device [12], which also used a Fiske-enhanced battery state (albeit at lower cell powers of only a few hundred nW compared to the tens of μW we use in this work), is ∼0.01 rad/day (Y. Sato, personal communications). This is consistent with the trend (in drift rate vs. cell power)

that we observe and suggests that lowering the battery power (by, for instance, using smaller size apertures) might lower the drift rate to previously observed values.

11 Conclusion

We have demonstrated the use of a continuously operating SHeQUID as a DC gyroscope. We have also flux locked this device by applying dynamic negative feedback and continuously tracked a varying rotation flux. We have also taken crucial first steps towards understanding the complex nature of the chemical potential battery, its interactions with cell resonances, and SHeQUID phase drifts stemming from battery operation.

Acknowledgements This work was supported by the National Science Foundation (DMR 0902147). Aperture arrays were fabricated at the Cornell Nanoscale Facility, a member of the National Nanotechnology Infrastructure Network, which is supported by the National Science Foundation (Grant ECS-0335765). They were cleaned and imaged in the Molecular Foundry at Lawrence Berkeley National Laboratory (supported by the Office of Science, Office of Basic Energy Sciences, of the U.S. Department of Energy under Contract No. DE-AC02-05CH11231). We are grateful for laboratory assistance by Yashwant Gowda and helpful discussions with Yuki Sato. We would also like to thank Michael Ray for joint previous work in exploring the dynamics of the chemical potential battery in a SHeQUID and for building and testing the high resolution thermometer that we use for temperature regulation.

References

1. Y. Sato, R.E. Packard, Rep. Prog. Phys. **75**, 016401 (2012)
2. A. Joshi, Y. Sato, R. Packard, J. Phys. Conf. Ser. **150**, 012018 (2009)
3. E. Hoskinson, Y. Sato, I. Hahn, R.E. Packard, Nat. Phys. **2**, 23 (2006)
4. H.A. Chan, M.V. Moody, H.J. Paik, Phys. Rev. D **35**, 3572 (1987)
5. L.A. Page, Phys. Rev. Lett. **35**, 543 (1975)
6. S.A. Werner, J.L. Staudenmann, R. Colella, Phys. Rev. Lett. **42**, 1103 (1979)
7. Y. Sato, A. Joshi, R. Packard, Phys. Rev. Lett. **98**, 195302 (2007)
8. Y. Sato, A. Joshi, R. Packard, Appl. Phys. Lett. **91**, 074107 (2007)
9. D.R. Tilley, J. Tilley, *Superfluidity and Superconductivity*, 3rd edn. (Institute of Physics, Bristol and Philadelphia, 1990), pp. 79–80
10. E. Hoskinson, R.E. Packard, T.M. Haard, Nature **433**, 376 (2005)
11. E. Hoskinson, R.E. Packard, Phys. Rev. Lett. **94**, 155303 (2005)
12. Y. Sato, Phys. Rev. B **81**, 172502 (2010)
13. E. Hoskinson, Y. Sato, K. Penanen, R.E. Packard, AIP Conf. Proc. **850**, 117 (2006)
14. K. Penanen, T. Chui, in *APS March Meeting*, L15.007 (2004)
15. D.D. Coon, M.D. Fiske, Phys. Rev. **138**, A744 (1965)
16. R.W. Simmonds, A. Loshak, A. Marchenkov, S. Backhaus, S. Pereversev, S. Vitale, J.C. Davis, R.E. Packard, Phys. Rev. Lett. **81**, 1247 (1998)
17. R.W. Simmonds Ph.D. thesis, University of California at Berkeley (2002), p. 139
18. O. Avenel, P. Hakonen, E. Varoquaux, Phys. Rev. Lett. **78**, 3602 (1997)
19. Y. Sato, R. Packard, Physica E **43**, 702 (2011)
20. S. Narayana, Y. Sato, Phys. Rev. Lett. **106**, 255301 (2011)
21. Y. Sato, A. Joshi, R. Packard, Phys. Rev. B **76**, 052505 (2007)
22. Y. Sato, A. Joshi, R. Packard, Phys. Rev. Lett. **101**, 085302 (2008)